Increased activity of the Vesicular Soluble N -Ethylmaleimide-sensitive Factor Attachment Protein Receptor TI-VAMP/VAMP7 by Tyrosine Phosphorylation in the Longin Domain

Andrea Burgo, Alessandra Casano, Aurelia Kuster, Stefan Arold, Guan Wang, Sébastien Nola, Agathe Verraes, Florent Dingli, Damarys Loew, Thierry Galli

THE JOURNAL OF BIOLOGICAL CHEMISTRY VOL. 288, NO. 17, pp. 11960–11972, April 26, 2013

Increased activity of the Vesicular Soluble *N*-Ethylmaleimide-sensitive Factor Attachment Protein Receptor TI-VAMP/VAMP7 by Tyrosine Phosphorylation in the Longin Domain*[S]

Received for publication, August 31, 2012, and in revised form, February 15, 2013 Published, JBC Papers in Press, March 7, 2013, DOI 10.1074/jbc.M112.415075

Andrea Burgo[‡§1,2], Alessandra M. Casano[‡§1,3], Aurelia Kuster[‡§1,4], Stefan T. Arold[¶], Guan Wang[‡§], Sébastien Nola[‡§], Agathe Verraes[‡§], Florent Dingli[‖], Damarys Loew[‖], and Thierry Galli[‡§5]

From the [‡]Institut Jacques Monod, UMR 7592, CNRS, Université Paris Diderot, Sorbonne Paris Cité, F-75013 Paris, France, [§]INSERM ERL U950, Membrane Traffic in Neuronal & Epithelial Morphogenesis, F-75013 Paris, France, the [¶]Department of Biochemistry and Molecular Biology, Center for Biomolecular Structure and Function, The University of Texas M. D. Anderson Cancer Center, Houston, Texas 77030, and the [‖]Institut Curie, Centre de Recherche, Laboratoire de Spectrométrie de Masse Protéomique, 75005 Paris, France

Background: The mechanism of activation of Longin vesicular SNAREs, particularly TI-VAMP/VAMP7, which is autoinhibited by its Longin domain, is largely unknown.
Results: Mimicking tyrosine 45 phosphorylation activates both t-SNARE binding and exocytosis of TI-VAMP.
Conclusion: TI-VAMP is positively regulated by tyrosine phosphorylation of the Longin domain.
Significance: Exocytosis mediated by TI-VAMP can be regulated by release of Longin domain autoinhibition.

Vesicular (v)- and target (t)-SNAREs play essential roles in intracellular membrane fusion through the formation of cytoplasmic α-helical bundles. Several v-SNAREs have a Longin N-terminal extension that, by promoting a closed conformation, plays an autoinhibitory function and decreases SNARE complex formation and membrane fusion efficiency. The molecular mechanism leading to Longin v-SNARE activation is largely unknown. Here we find that exocytosis mediated by the Longin v-SNARE TI-VAMP/VAMP7 is activated by tonic treatment with insulin and insulin-like growth factor-1 but not by depolarization and intracellular calcium rise. In search of a potential downstream mechanism, we found that TI-VAMP is phosphorylated *in vitro* by c-Src kinase on tyrosine 45 of the Longin domain. Accordingly, a mutation of tyrosine 45 into glutamate, but not phenylalanine, activates both t-SNARE binding and exocytosis. Activation of TI-VAMP-mediated exocytosis thus relies on tyrosine phosphorylation.

Soluble *N*-ethylmaleimide-sensitive factor attachment protein receptors (SNAREs)[6] mediate intracellular membrane fusion in the secretory and endocytic pathways. Vesicular (v)- and target (t)-SNARE forms a so-called trans-SNARE complex or SNAREpin, which is required to merge the two membranes. v-SNAREs are classified in two main subfamilies: the "Brevin", which includes short v-SNAREs, and the "Longin", characterized by the Longin domain (LD) N-terminal extension of ~120 amino acids. The v-SNARE TI-VAMP/VAMP7 (TI-VAMP) is a prototypic Longin v-SNARE (1) and was previously shown to mediate exocytosis in several cell types (2) including neurons (3). TI-VAMP may be involved in neurotransmitter basal release (4, 5) and specific brain circuits and functions (6). In addition, TI-VAMP secretory vesicles release compounds like ATP in non-neuronal cells (7, 8) and other active compounds that depend on the cell type (2) and also transmembrane proteins like CD82 (9). The LD of TI-VAMP plays a role in autoinhibitory regulation of TI-VAMP exocytic activity by controlling its capacity to interact with plasma membrane t-SNARE partners (10–12). The LD of TI-VAMP consists of five antiparallel β-strands sandwiched by two α-helices on one side and one α-helix on the other (β1β2α1β3β4β5α2α3 topology) located at the N terminus of the protein. The native full-length cytoplasmic domain of TI-VAMP adopts a predominantly closed conformation with remarkable stability that requires at least the N-terminal 160 residues and is further stabilized by the C-terminal 20 residues preceding the transmembrane domain. In the LD of TI-VAMP, Leu-43 and Tyr-45 are included in the hydro-

* This work was supported by grants from INSERM, the Association Française contre les Myopathies, the Association pour la Recherche sur le Cancer, the Mairie de Paris Medical Research and Health Program, the Fondation pour la Recherche Médicale, the Ecole des Neurosciences de Paris (to T. G.).
[S] This article contains supplemental Movies S1–S3.
[1] These authors contributed equally to this work.
[2] Present address: Laboratoire Structure, Activité des Biomolécules Normales et Pathologiques, Université d'Evry Val-d'Essonne, Bat. Maupertuis, Rue du Père Jarlan, 91100 Evry.
[3] Present address: Peri Group, EMBL Heidelberg, Meyerhofstrasse 1, 69117 Heidelberg, Germany.
[4] Supported by a doctoral student fellowship from Association pour la Recherche sur le Cancer.
[5] To whom correspondence should be addressed: Inst. Jacques Monod, Bat. Buffon, 15 Rue Hélène Brion, 75205 Paris CEDEX 13, France. Tel.: 33-157-278-039; Fax: 33-157-278-036; E-mail: thierry.galli@inserm.fr.

[6] The abbreviations used are: SNARE, soluble *N*-ethylmaleimide-sensitive factor attachment protein receptor; v-SNARE, vesicular SNARE; t-SNARE, target SNARE; LD, Longin domain; DIV, days *in vitro*; pHL, pHluorin; IGF-1, insulin-like growth factor 1; IGF-1R, IGF-1 receptor; ANOVA, analysis of variance.

phobic pocket on the surface of the LD and play a crucial role to maintain a closed conformation in TI-VAMP (12).

The interaction between t-SNARE and v-SNARE proteins during membrane fusion is a sophisticated mechanism subjected to different levels of regulation that is achieved through the interaction of SNAREs with regulatory proteins (13). Recently, phosphorylation also appeared as a modulatory mechanism for the regulation of biological activity of SNAREs (14). Most commonly occurring on threonine, serine, and tyrosine residues, phosphorylation plays a critical role in the regulation of many cellular processes, among which is synaptic function (15). Given the chemical nature of the phosphate group, phosphorylation implies the insertion of a bulky negative charge in the protein structure, which often causes significant conformational changes. Several studies demonstrated that SNAREs and some of their regulators undergo dynamic conformational changes and that their biological activity is modulated by phosphorylation. For instance, treatment of PC12 cells with a PKC activator results in Ser phosphorylation of SNAP-25, which reduces its association with Syntaxin-1 (16). Syntaxin-1 is phosphorylated on Ser by casein kinase II with a direct effect on the mobility of secretory vesicles and their subsequent fusion competence (17). Here we reasoned that a reversible post-translational modification, such as phosphorylation, could lead to change in TI-VAMP structure and activate its function. We found that TI-VAMP exocytosis is regulated by long lasting treatment with insulin or insulin-like growth factor-1 (IGF-1) and that c-Src kinase is involved in the Tyr-45 phosphorylation of the LD of TI-VAMP. Furthermore, we demonstrated that the Tyr-45 mutation in Glu of TI-VAMP is more active for plasma membrane t-SNARE binding. This modification further promotes axonal growth and TI-VAMP-mediated exocytosis in hippocampal neurons.

EXPERIMENTAL PROCEDURES

Antibodies and cDNA Constructs—The mouse mAb against GFP was from Roche Diagnostics. Chicken anti-MAP2 antibody was from Abcam. Rabbit polyclonal antibodies anti-RFP and mouse mAb anti-Tau were from Chemicon. Mouse mAb against β-tubulin was from The Hybridoma Bank (clone E7). Aspecific rabbit IgG immunoglobulins were from Sigma-Aldrich. For the detection of tyrosine phosphorylation, we used the mouse mAb 4G10® Platinum (Millipore) against phosphotyrosine. Rabbit polyclonal antibodies anti-GFP, anti-TI-VAMP (TG50), and the mouse mAb anti-TI-VAMP (clone 158.2) were described previously (18, 19). The mouse mAb against SNAP-25 (71.1) was from Reinhard Jahn (Max Planck Institute, Gottingen, Germany). Mouse mAb against Syntaxin-1 (HPC1) was a generous gift from C. Barnstable (Yale University, New Haven, CT). Rabbit anti-c-Src was purchased from Santa Cruz.

GFP-, mRFP-, and pHL-tagged forms of TI-VAMP-WT were described previously (3, 18). Sequences encoding amino acids 1–124 were deleted from TI-VAMP-WT to create TI-VAMP-ΔLD by using PCR and the following sets of oligonucleotides: 5′-ATGGTGACGGAGACTCAAGCC-3′ and 5′-GGTTTATTTGTATAGTTCATCCATGCC-3′. The Y45F and Y45E mutations were obtained by site-directed mutagenesis of both GFP- and -pHL-TI-VAMP-WT constructs using the QuikChange® site-directed mutagenesis kit protocol (Stratagene) and the following sets of oligonucleotides: 5′-CTGAAAATAATAAACTAACTTTCTCTCATGGCAATTATTTG-3′ and 5′-CAAATAATTGCCATGAGAGAAAGTTAGTTTATTATTTTCAG-3′ for the Y45F mutant; 5′-CTGAAAATAATAAACTAACTGAGTCTCATGGCAATTATTTG-3′ and 5′-CAAATAATTGCCATGAGACTCAGTTAGTTTATTATTTTCG-3′ for the Y45E mutant. The c-Src Y530F and c-Src Y419F plasmids were a generous gift from Michele Sallese (Unit of Genomic Approaches to Membrane Traffic, Chieti, Italy).

In Vitro Phosphorylation of TI-VAMP, Trypsin Digestion, and Mass Spectrometry—The fragments His_6-LD human TI-VAMP (amino acids 1–127) and His_6-Cyto TI-VAMP (amino acids 1–190) were cloned in pET-46 Ek/LIC, expressed in the BL21(DE3) *Escherichia coli* strain, and purified as described previously (20). Purified fragments (2 μg) were incubated at 30 °C for 1 h without (control −Src) or with 100 ng of recombinant Src (expressed and purified in Sf21 insect cells from Merck Millipore Corporation) in 30 μl of reaction buffer (100 mM Tris-HCl, pH 7.2, 125 mM $MgCl_2$, 2 mM EGTA, 2.5 mM ATP, 0.25 mM orthovanadate, 1 mM NaF, 2 mM DTT) supplemented with phosphatase and protease inhibitors (PhosStop, Complete EDTA free; Roche Diagnostics). The reaction was terminated by addition of SDS-protein loading buffer and boiled at 95 °C for 10 min. The samples were separated by SDS-PAGE. In gel digests were performed as described in standard protocols. Briefly, following SDS-PAGE and washing of the excised gel slices proteins were reduced by adding DTT (Sigma-Aldrich) prior to alkylation with iodoacetamide (Sigma-Aldrich). After washing and shrinking of the gel pieces with 100% acetonitrile, trypsin (sequencing grade modified; Promega) was added, and the proteins were digested overnight as described previously (21). For phosphopeptide analysis, the probes were directly used for nanoLC-MS/MS. The samples were separated on a C18 reversed phase column (75 μm inner diameter × 15 or 50 cm, packed with C18 Acclaim PepMap™, 3 μm, 100 Å; LC Packings) via a 60-min (or via a 150-min) linear acetonitrile gradient (UltiMate 3000 system; Dionex) before MS and MS/MS. The spectra were recorded on an LTQ Orbitrap XL™ mass spectrometer (Thermo Scientific). The mass spectrometer was set to acquire a single MS scan followed by up to five data-dependent scans and, if a neutral loss of 98 Da from the precursor ion was observed in the collision-induced dissociation mass spectrum, an MS3 scan of the neutral loss ion (simultaneous fragmentation of neutral loss product and precursor was enabled, dynamic exclusion repeat count of 1, repeat duration of 30 s, exclusion duration of 180 s, and lock mass option was enabled). The resulting spectra were then analyzed via the Mascot™ and the SEQUEST® software (Matrix Science and Thermo Scientific) created with Proteome Discoverer (version 1.3, Thermo Scientific) using an in-house database containing the human TI-VAMP protein (P51809, UniProtKB/Swiss-Prot, description: vesicle-associated membrane protein 7). All phosphorylated peptides that have their nonphosphorylated counterparts were manually validated.

Cell Culture, Cell Transfection, and Reagents—COS-7 and HeLa cells were grown in DMEM (Invitrogen) containing 10%

(v/v) FBS (PAA Laboratories), 10 units/ml penicillin, and 10 μg/ml streptomycin in a 5% CO_2-humidified atmosphere at 37 °C. Hippocampal neurons from embryonic rats (embryonic day 19) were prepared as described previously (22) and grown on polyornithine-coated (Sigma-Aldrich) either 14- or 30-mm coverslips at a density of 100,000 and 500,000, respectively in Neurobasal medium supplemented with 2% B27, 2 mM L-glutamine. For interaction assays and co-localization experiments, COS-7 or HeLa cells were transfected by electroporation as follows: 7×10^6 cells were centrifuged (800 rpm, 5 min, 25 °C), washed once with room temperature serum free-DMEM, and washed once with Cytomix solution (25 mM HEPES, 120 mM KCl, 10 mM KH_2PO_4, 0.15 mM $CaCl_2$, 5 mM $MgCl_2$, 2 mM EGTA, pH 7.6). The cells were then resuspended in 0.5 ml of Cytomix solution and treated with both 2 mM ATP and 5 mM glutathione. After the addition of 20 μg (HeLa) or 35 μg (COS-7) of plasmids, the cells were electroporated (0.25 kV for HeLa, 0.29 kV for COS-7, 1000 microfarads) and plated on dishes of 10 cm of diameter or glass coverslips. For TI-VAMP phosphorylation assay, COS-7 cells were transfected with 25 μg of both c-Src plasmids and TI-VAMP-pHL constructs. The cells were processed for the different analysis 24 h after transfection. For the video imaging, surface staining and axonal length experiments COS-7 cells and 2 DIV rat hippocampal neurons were transfected by using Lipofectamine 2000 (Invitrogen) according to the manufacturer's instructions. 16–24 h after transfection, the cells were imaged live or fixed with 4% paraformaldehyde and processed for immunofluorescence. Alternatively rat hippocampal neurons were transfected at 7 DIV using calcium phosphate method (CalPhos; Clontech) and analyzed after 16–24 h. Insulin from bovine pancreas was from Sigma-Aldrich, IGF-1 rat recombinant protein from GenWay Biotech, brain-derived neurotrophic growth factor from U.S. Biological, wortmannin, bryostatin, phorbol 12-myristate 13-acetate, 8-bromoadenosine-cAMP, dybutyril-cAMP, forskolin, SB415286, and 8-bromoguanosine-cGMP were from Tocris Bioscience.

Structural Analysis—Structural analysis of TI-VAMP was based on the crystal structure of the LD bound to Hrb (Protein Data Bank code 2VX8 (23)) and on the crystal structure of TI-VAMP in its closed autoinhibitory conformation bound to Varp (Protein Data Bank code 4B93 (24)). Structural models for phosphorylated Tyr-45 were built by replacing Tyr-45 with Tyr(P) in the structure, followed by mild energy minimization by Refmac (25).

Immunofluorescence Staining and Axonal Length Assay—For the surface immunostaining, COS-7 cells were plated on polyornithine-coated coverslips and treated 24 h after transfection as described previously (3). Briefly, the cells were washed at 4 °C with DMEM buffered with 20 mM HEPES and then incubated 5 min at 4 °C with mouse mAb anti-GFP. After extensive washing, the cells were fixed and incubated with a Cy3-coupled secondary antibody. The cells were then permeabilized and processed for immunofluorescence using the same primary antibody and the Alexa Fluor 488-coupled secondary antibody. This protocol allowed to determination of the fraction of TI-VAMP expressed at the surface (Cy3 staining) and the total amount of expressed protein (Alexa Fluor 488 staining). For quantification of the ratio between surface (red channel)/total (green channel) integrated signals, between 35 and 68 TI-VAMPs pHL-expressing cells were considered. Images were acquired with a Leica DMRA2 upright microscope (Leica Microsystems, Manheimm, Germany) equipped with a CoolSNAP ES CCD camera (Photometrics, Roper Scientific, Trenton, NJ) and a Leica HCX PL APO 40×/1.25–1.75 NA CS oil immersion objective.

For indirect immunofluorescence, the cells were fixed 16–24 h after transfection and processed as described previously (10). The images of HeLa cells were obtained using a confocal microscope (TCS SP5; Leica Microsystems) and an oil immersion 100× objective with sequential acquisition settings of 1024 × 1024 pixels. For axonal length assay in rat hippocampal neurons, between 20 and 30 transfected neurons were randomly selected, and the axon, defined as the longest and MAP2-negative neurites, was measured by using Metamorph software (Roper Scientific). Each experiment was repeated three times with similar results. Statistical significance was determined by using GraphPad Prism 5 software.

Immunoprecipitation and Immunoblot Assays—Immunoprecipitation experiments were carried out as described previously (11). Briefly, the cells were lysed in TSE (50 mM Tris-HCl, pH 8.0, 150 mM NaCl, 1 mM EDTA) supplemented with 1% Triton X-100 and Complete tablet (Roche Diagnostics). For TI-VAMP phosphorylation assay, lysis buffer was supplemented with PhosStop tablet (Roche Diagnostics). 1 mg of protein extract was submitted to immunoprecipitation overnight at 4 °C, with 50 μl of protein G-coupled Sepharose beads (GE Healthcare) previously cross-linked with the specific antibody. After specific wash, bound proteins were eluted with 30 μl of glycine 50 mM + Triton X-100 2% (pH 2.5) and treated with 3 μl of Tris 1 M (pH 8.0). Eluted proteins were processed for SDS-PAGE analysis by using 15% homemade SDS gels or NuPAGE 4–12% Bis-Tris gradient gels (Applied Biosystems). The gels were run in Tris-glycine electrophoresis buffer (25 mM Tris, 250 mM glycine, 0.1% SDS), MOPS or MES buffers (Invitrogen), transferred onto nitrocellulose filters (Protran), and then processed for Western blotting. The membranes were blocked with 5% BSA in TBST (200 mM Tris, 150 mM NaCl, 0.1% Tween 20, pH 7.3) followed by incubation with the primary antibodies overnight. After washing, the membranes were blotted with secondary antibodies, and detection was carried out by the infrared imaging system Odyssey of LI-COR Biosciences.

Time Lapse Imaging—COS-7 cells and primary hippocampal neurons were cultured on 30-mm diameter glass coverslips. Optical recordings were performed between 16 and 24 h after transfection. For pHluorin acquisition, the images were recorded every 0.5 s over a time period of 3 min, by using a 488-Ar^+ ion acousto-optically shuttered laser whose beam was expanded to fill the field of view, an inverted microscope Leica DMI6000B (Leica Microsystems), a 63×/1.4 NA Plan-Apochromat oil immersion Leica objective, a 1.6× tube lens with 497–557-nm emission and 505-nm dichroic filters and digital camera (Cascade:512B; Roper Scientific, Trenton, NJ) as described previously (3). Imaging was conducted in modified Krebs-Ringer-HEPES buffer (135 mM NaCl, 2.5 mM KCl, 1.2 mM $MgCl_2$, 1 mM $CaCl_2$, 20 mM HEPES, 11.1 mM glucose, and

TABLE 1

Analysis of TI-VAMP exocytosis in rat hippocampal neurons at 3 DIV

Rat hippocampal neurons in culture were transfected at 2 DIV with TI-VAMP-WT pHL. The neurons were then treated with the drugs indicated in the table and imaged live at 3 DIV to analyze the exocytic events in the cell body. The effect of intracellular Ca^{2+} changes in TI-VAMP exocytosis were also analyzed either by 40 mM KCl depolarization or by electrical stimulation.

Drugs	Concentration and compounds
PI3K inhibitor	1 μM wortmannin
PKC activators	100 nM bryostatin, 1 μM phorbol 12-myristate 13-acetate
cAMP analogues	1 mM 8-bromoadenosine-cAMP, 1 mM dybutyril-cAMP
Adenylate cyclase activator	10–20 μM forskolin
GSK-3 inhibitor	20 μM SB415286
cGMP analogue	100 μM 8-bromoguanosine-cGMP
Growth factor	50–100 ng/ml brain-derived neurotrophic growth factor
Ca^{2+} signaling	K^+ depolarization, electrical stimulation

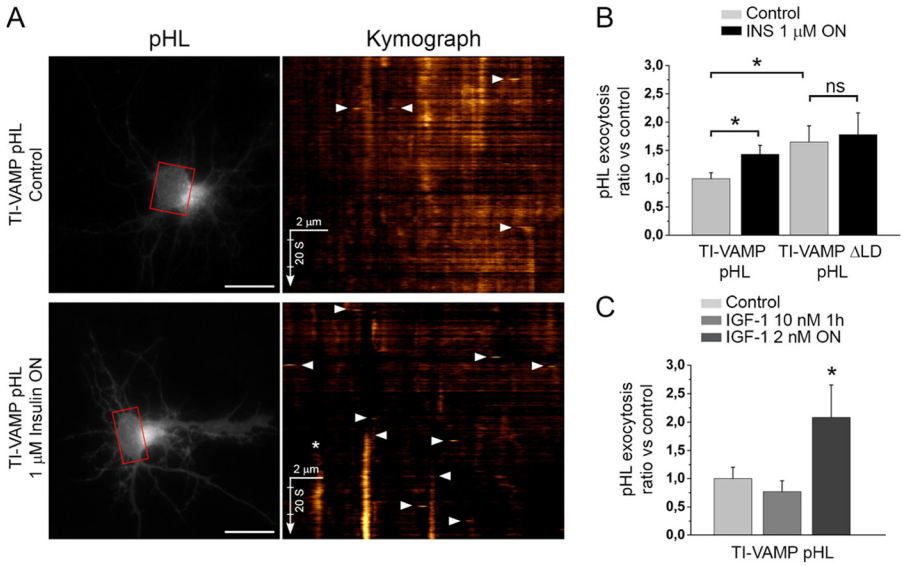

FIGURE 1. **TI-VAMP exocytosis is activated by insulin/IGF-1 cell treatment.** *A*, rat hippocampal neurons were transfected at 2 DIV with TI-VAMP-WT or -ΔLD and treated, or not, overnight with 1 μM insulin (*INS*). The neurons were then imaged live at 3 DIV, and the exocytic events of TI-VAMP pHL constructs in the cell body (in *red boxes*) were quantified as described under "Experimental Procedures." The more relevant exocytic events, here visualized by kymograph (see also supplemental Movie S1), appear as bright spots (*arrowheads*). *, exocytic event not quantified. *Scale bars*, 20 μm (*left panels*). *B*, quantification of exocytic events of TI-VAMP pHL constructs. *C*, rat hippocampal neurons were transfected at 2 or 7 DIV with TI-VAMP-WT and left untreated or treated for 1 h or overnight with IGF-1. The neurons were then imaged, and exocytic events of TI-VAMP pHL in the cell body were quantified as described above. The data are represented as ratios between the densities per second of exocytic events of TI-VAMP-WT or -ΔLD treated cells and TI-VAMP-WT untreated cells. The data are shown as the means ± S.E. Significance was determined by one-way ANOVA, Dunnett's post test. *, $p < 0.05$; *ns*, not significant.

TABLE 2

Predicted sites of Tyr phosphorylation in the TI-VAMP sequence

Indications about possible Tyr phosphorylation of TI-VAMP were obtained through bioinformatic predictions on the *Rattus norvegicus* TI-VAMP protein sequence using web phospho prediction software. c-Src, nonreceptor tyrosine kinase c-Src; IR, insulin receptor; Jak, Janus kinase; EGFR, epidermal growth factor receptor; hprd, human protein reference database (47); kphos, Kinase Phosp (48) with prediction specificity of 95%); Netphos, Netphos 2.0 server (49); Netphosk, NetPhosK 1.0 server with a threshold of 0.5 (50); GPS2.1, group-based prediction system (51).

	Tyr-45	Tyr-50	Tyr-54	Tyr-62	Tyr-90	Tyr-100	Tyr-202
hprd	+ (c-Src)			+ (c-Src)	+ (c-Src)	+ (c-Src)	+ (Jak2)
kphos (95%)	+ (IR)		+ (IR)				+ (Jak)
Netphos	+	+			+	+	
Netphosk	+ (IR)						+ (EGFR)
GPS2.1	+ (c-Src)			+ (c-Src)		+ (c-Src)	+ (c-Src)

pH 7.4). Exocytic events of TI-VAMP pHL in hippocampal neurons and COS-7 cells were manually counted by using the ImageJ plugin Point Picker and related to the analyzed cell surface area (expressed in μm^2) and the time of recording (180 s). For COS-7 cells TI-VAMP-pHluorin exocytic events were also detected automatically using custom-written scripts in FIJI and Matlab software. Briefly, time lapse stacks were processed to reveal all sudden appearance of fluorescent spots in FIJI. Average intensity of fluorescence was measured in a 5 × 5-pixel region of interest centered on each spot for each slice. Fluorescent traces were then analyzed and filtered in Matlab. Events were defined as a transient increase of fluorescence followed by an exponential decay to base line. Duration of events was defined as the time between the image where the spot appear and the image where fluorescence trace fell below base line. Exocytic events are represented in Figs. 1*A*, 5*C*, and 8*C* using kymographs. A narrow box delimitating the soma of the neuron or a smaller region in the soma of COS-7 cells was drawn, and the kymograph image was created using the kymograph application in the Metamorph program (Molecular Devices, Roper

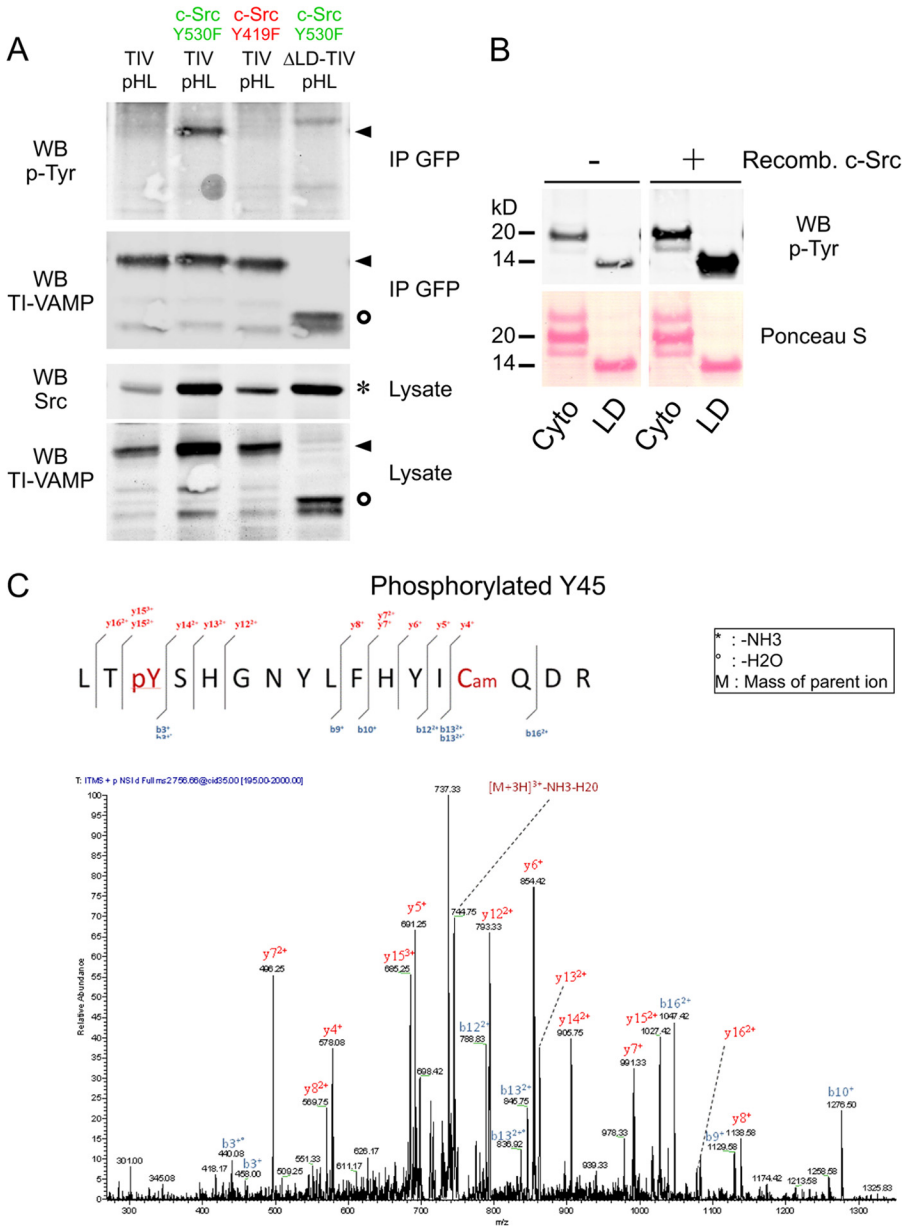

FIGURE 2. **TI-VAMP is phosphorylated by c-Src.** *A*, COS-7 cells were co-transfected with TI-VAMP-WT pHL and Src either in constitutive activated (c-Src Y530F) or inactivated (c-Src Y419F) form. The cells were also transfected with TI-VAMP-WT pHL alone or co-transfected with TI-VAMP-ΔLD pHL and c-Src Y530F as controls. After 16–24 h, the proteins were extracted, and immunoprecipitation (*IP*) was performed by using monoclonal antibody against GFP. The degree of phosphorylation of TI-VAMP was assessed by using anti-phosphotyrosine antibody 4G10. *Circles*, TI-VAMP-ΔLD pHL; *arrowheads*, TI-VAMP-WT pHL; *asterisk*, c-Src. *B*, phosphorylation of TI-VAMP *in vitro*. Recombinant (*Recomb.*) cytoplasmic domain (*Cyto*) and Longin domain (*LD*) of TI-VAMP were phosphorylated *in vitro* by purified c-Src kinase. Each reaction contained equivalent amounts of Cyto and LD proteins as assessed by Ponceau S Red staining. Src-phosphorylated proteins were detected by Western blotting (*WB*) using an antibody against phosphotyrosine residues (*p-Tyr*). *C*, representative MS/MS spectrum (simultaneous fragmentation of neutral loss product and precursor) for identification of TI-VAMP phosphorylation site and LC electrospray ionization MS/MS spectrum for a carbamidomethylated peptide, with the position of the phosphate group LTpY^{45}SHGNYLFHYICamQDR (756.6$^{(3+)}$ *m/z*). The fragmentation spectrum derived from trypsin TI-VAMP peptide is shown. The *inset* shows the peptide sequence and the observed ions obtained from the phospho-peptide. Tandem mass spectrum labeled to show singly and doubly charged *b* and *y* ions, as well as ion corresponding to neutral losses of water (*circles*) and NH_3 (*asterisks*); *M*, parent ion mass. *TIV*, TI-VAMP.

Scientific SAS, Evry, France). In these kymographs, the *y* axis represents the time, and the *x* axis represents the maximum intensity value from the pixels along the box. Transient exocytic events appear as bright spots, whereas long lasting exocytosis as irregular bright lines lasting over time. KCl-induced depolarization was conducted by substituting 40 mM NaCl in the modified Krebs-Ringer-HEPES buffer with 40 mM KCl, with all other components remaining unchanged. For field electrical depolarization, the neurons were imaged in a closed bath chamber (RC-21BRFS; Warner Instruments) and electrical stimulation with a frequency of 10 Hz (pulse duration, 10 ms; intensity, 30 mA as a bipolar square wave current output) were applied for 30 s by a stimulator (Stimulus Isolator A385; WPI) equipped with a pulse generator (Accupulser A310; WPI).

Vesicle Analysis—The images were deconvolved using the two-dimensional spectral deconvolution plugin from the "MacBiophotonics" version of ImageJ and then thresholded to select vesicles. The resulting binary mask was then applied to

the original images, so vesicles were segmented, and the original gray values were conserved. The number and the area of single vesicle in each cell were then evaluated by the "analyze particles" command. Cell area was estimated by intensity thresholding of the original images. For each cell, vesicle density was calculating by dividing the total number of vesicles with the corresponding cell area. Statistical significance was estimated using GraphPad Prism 5 software.

In Vitro Interaction Assays—For *in vitro* interaction assays, an *E. coli* stra2in co-expressing GST-Syntaxin-1 and His_6-SNAP-25 was kindly provided by G. Schiavo (Cancer Research UK, London, UK). Purification of the recombinant complex was performed as described previously (26). The GFP-TI-VAMP constructs (-WT, -ΔLD, -Y45E, and -Y45F) and GFP alone were transfected in COS-7 cells with 35 μg of the encoding DNA plasmid. After cell lysis, the fluorescence (λ_{ex} = 488 nm, λ_{em} = 500–550 nm) of the extracts was quantified to include equal amounts of GFP-tagged proteins in the *in vitro* interaction assay. After overnight incubation of the protein lysate with the glutathione beads coated with the GST-Syntaxin1/His_6-SNAP-25 SNARE complex at 4 °C, samples were loaded on a 15% SDS-PAGE gels and processed for Western blotting. The GFP fusion proteins bound to the SNARE complex were quantified for each condition with ImageJ software, and the ratio between the pulled down proteins and their level of expression in the lysates was considered. The same experiment was repeated three times with similar results.

RESULTS

TI-VAMP Is Phosphorylated by c-Src—To identify signaling compounds that could regulate TI-VAMP exocytosis, we analyzed by fast time lapse video imaging the effect of pharmacological treatments in cultured rat hippocampal neurons expressing TI-VAMP-WT fused in the luminal domain to a pH-sensitive GFP, so-called pHluorin (pHL) (27). This method allowed us to show that TI-VAMP vesicles exocytose spontaneously in developing neurons (3, 28). Inhibition or activation of molecules implicated in axon specification and guidance, such as those acting on PI3K, PKC, adenylate cyclase, and GSK-3 or raising intracellular cAMP or cGMP, did not affect TI-VAMP exocytosis (Table 1). Neither stimulation with brain-derived neurotrophic growth factor nor depolarization with KCl 40 mM and electrical stimulation affected TI-VAMP exocytosis in hippocampal neurons at 3 DIV (Table 1). In contrast, overnight stimulation of the insulin receptor with 1 μM insulin increased exocytosis of TI-VAMP-WT but not TI-VAMP lacking the LD (−ΔLD) pHL (Fig. 1, *A* and *B*, and supplemental Movie S1). However, short insulin treatment (5–20 min) did not affect TI-VAMP-WT exocytosis (data not shown). Furthermore, the long lasting treatment of hippocampal neurons with 2 nM IGF-1, which has higher affinity for IGF-1 receptor (IGF-1R) than insulin receptor (29), significantly increased the rate of TI-VAMP-WT exocytosis (Fig. 1*C*). Interestingly, TI-VAMP mediates 30% of the gain in plasma membrane surface of GLUT4 transport in response to insulin stimulation in muscle cells (30). Both insulin receptor and IGF-1R are receptor tyrosine kinases that regulate several brain and neuronal functions, including neurite growth (31–34). Bioinformatic predictions of

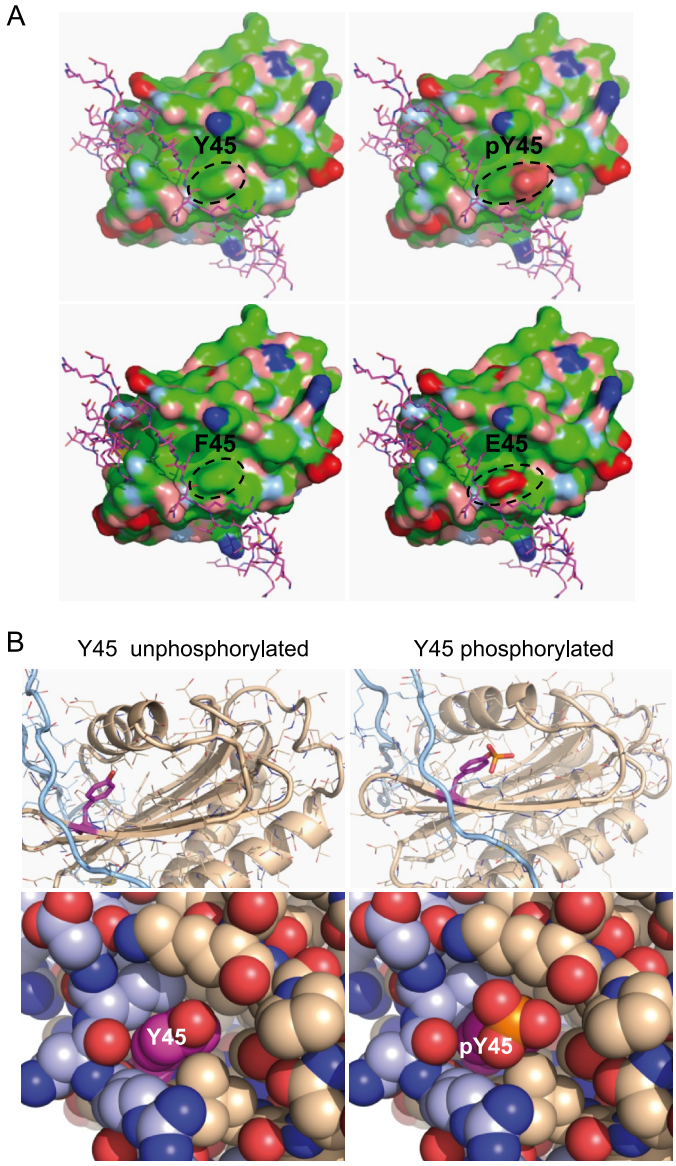

FIGURE 3. **Modeling of Tyr(P)-45 TI-VAMP.** *A*, molecular surface of the TI-VAMP LD (Protein Data Bank code 4B93 (24)). *Blue*, positively charged atoms; *red*, negatively charged atoms; *green*, hydrophobic atoms; *salmon*, polar oxygens; *light blue*, polar nitrogens; *yellow*, sulfur. The SNARE motif (*magenta stick model*) is shown in its autoinhibitory interaction with LD. The *top right panel* shows that phosphorylation of Tyr-45 (*outlined*) adds a bulky charge to the center of a shallow hydrophobic groove. The unphosphorylated molecule is shown for comparison in the *top left panel*. The *bottom panels* show homology models for the Y45F and Y45E mutants. *B*, Tyr-45 (*magenta*) of the LD (*beige*) is situated in the binding region for the SNARE motif (*light blue*). *Left panels*, Tyr-45 crystal structure 4B93; *right panels*, Tyr(P)-45 homology model. *Top panels*, ribbon and stick representation; *bottom panels*, atoms are shown as van der Waals spheres. Phosphorylation of Tyr-45 introduces a bulky charge in this interaction site, potentially altering ligand interactions (*right panels*).

phosphorylation of TI-VAMP (Table 2) suggested that several tyrosine residues in the LD, particularly Tyr-45, could be phosphorylated. This was interesting because Tyr-45 appeared as a key residue for the interaction between the LD and the SNARE core of TI-VAMP (12). Moreover, Tyr-45 was predicted to be potentially phosphorylated by c-Src, a cytosolic nonreceptor tyrosine kinase involved in many cell functions, some of which are downstream insulin receptor and IGF-1R (35, 36). Furthermore, it has been shown that inhibition of c-Src decreases the frequency of

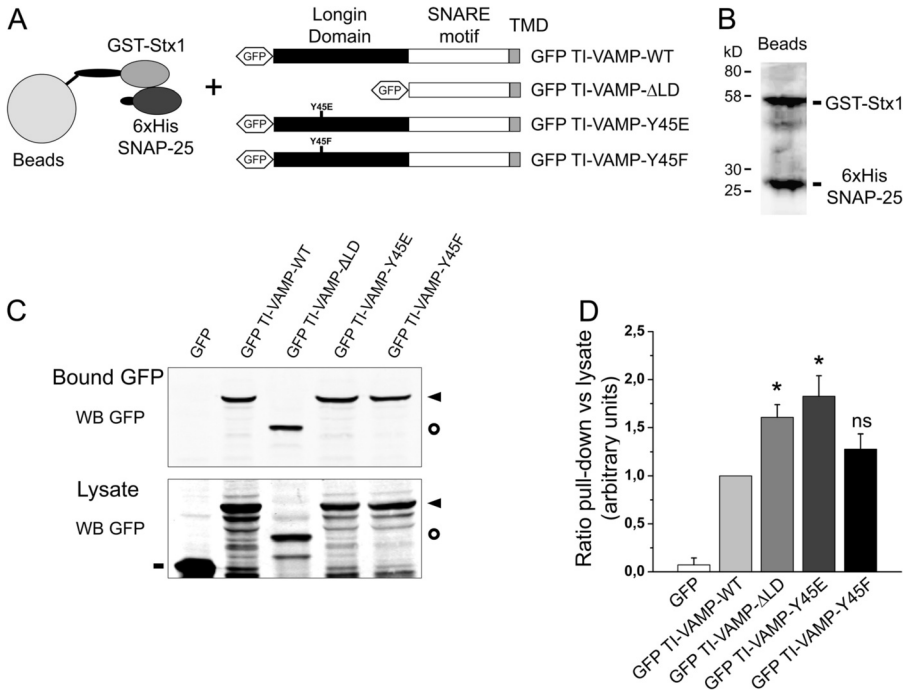

FIGURE 4. **The *in vitro* interaction of TI-VAMP with its molecular partners depends on tyrosine phosphorylation.** Quantitative *in vitro* assay to measure the interaction between recombinant Stx1/SNAP-25 and TI-VAMP mutants. *A*, COS-7 cells were transfected with GFP alone or GFP-TI-VAMP-WT, -ΔLD, -Y45E, or -Y45F. After 16–24 h, the proteins were extracted and incubated with recombinant t-SNARE complex composed of GST-Stx1 and His_6-SNAP-25 immobilized on glutathione beads. *TMD*, transmembrane domain. *B*, Coomassie Blue staining of purified recombinant GST-Stx1 and His_6-SNAP-25 immobilized on beads. *C*, Western blots (*WB*) showing bound GFP fusion proteins eluted from the beads (*upper panel*) and their expression in the lysates (*lower panel*). *D*, quantification of the binding affinity of GFP TI-VAMP (WT and mutated forms) to the recombinant partners. The ratio between each bound GFP fusion protein (pulldown) and its respective expression in the cell lysate is considered. The data are shown as the means ± S.E. Significance was determined by one-way ANOVA, Dunnett's post test. *, $p < 0.05$; *ns*, not significant. *Circles*, GFP TI-VAMP-ΔLD; *dashes*, GFP; *arrowheads*, GFP-TI-VAMP-WT, -Y45E, and -Y45F.

TI-VAMP exocytic events in cortical neurons (28), suggesting that TI-VAMP is downstream of c-Src activity. Altogether, this evidence suggested that c-Src could phosphorylate TI-VAMP.

To analyze the role of c-Src in Tyr phosphorylation of TI-VAMP, COS-7 cells were co-transfected with both TI-VAMP-WT pHL and c-Src, either in constitutive active (c-Src Y530F) or inactive (c-Src Y419F) form (37, 38). TI-VAMP lacking the LD and therefore all the Tyr residues in the first 100 amino acids was also co-expressed with c-Src Y530F, as positive control. After pHL immunoprecipitation, the degree of Tyr phosphorylation of TI-VAMP was assessed using specific Tyr(P) detection of immunoprecipitated TI-VAMP by Western blotting. We found that TI-VAMP-WT co-expressed with c-Src Y530F but not c-Src Y419F was Tyr-phosphorylated (Fig. 2*A*). Furthermore, TI-VAMP-ΔLD was not phosphorylated by c-Src Y530F, suggesting that this phosphorylation occurred specifically in the LD. As control, expression of both an active and an inactive form of c-Src tyrosine kinase, a c-Src negative regulator (39), did not induce Tyr phosphorylation of TI-VAMP-WT (data not shown).

To precisely determine the Tyr residues that c-Src could phosphorylate in the LD, we incubated recombinant c-Src with purified LD or purified full-length TI-VAMP deleted of transmembrane domain (Cyto). We found that purified LD was phosphorylated by recombinant c-Src (Fig. 2*B*). Purified Cyto was also phosphorylated but to a lesser extent in agreement with a less accessible Tyr residues when the SNARE domain folds over the LD. The LD phosphorylated protein was then digested with trypsin and analyzed by liquid chromatography coupled to electrospray tandem mass spectrometry. We found that Tyr-45 was phosphorylated by c-Src *in vitro* (Fig. 2*C*). Structural analysis of TI-VAMP suggested that Tyr-45 is solvent-exposed on the β3 strand of the central β-sheet of the LD, within a large hydrophobic patch (Fig. 3*A*). Tyr-45 contributes significantly to both binding of Hrb, AP-3δ, and the intramolecular SNARE/longin interaction (12, 23, 24, 40). Phosphorylation of Tyr-45 will introduce a bulky charged moiety into this hydrophobic binding region, significantly altering the shape and electrostatic characteristics of this surface (Fig. 3). Thus, phosphorylation of Tyr-45 would be well positioned to alter binding interactions of this region, including the intramolecular SNARE binding (12).

Y45E Mutation Increases the Binding of TI-VAMP with t-SNAREs—To get insight into the role of Tyr-45 phosphorylation, we substituted this residue with glutamate or phenylalanine, because this approach is classically used to mimic phosphorylated and unphosphorylated forms of the protein at that position respectively (Fig. 3*A*). The wild type form (WT), Y45E mutant (Y45E), Y45F mutant (Y45F), and TI-VAMP-ΔLD were fused to N-terminal GFP or C-terminal pHL tag. To understand whether or not Tyr-45 mutation regulates the activity of TI-VAMP, we measured the binding of TI-VAMP mutants to its plasma membrane t-SNARE partners (Syntaxin-1 and SNAP-25) *in vitro*, as described previously (11) (Fig. 4, *A* and *B*). The Y45E mutation, but not Y45F, increased the interaction of TI-VAMP with immobilized t-SNAREs, and this effect was similar to the deletion of the LD (11) (Fig. 4, *C* and *D*). Taken together, these results show that the interaction of TI-VAMP with its

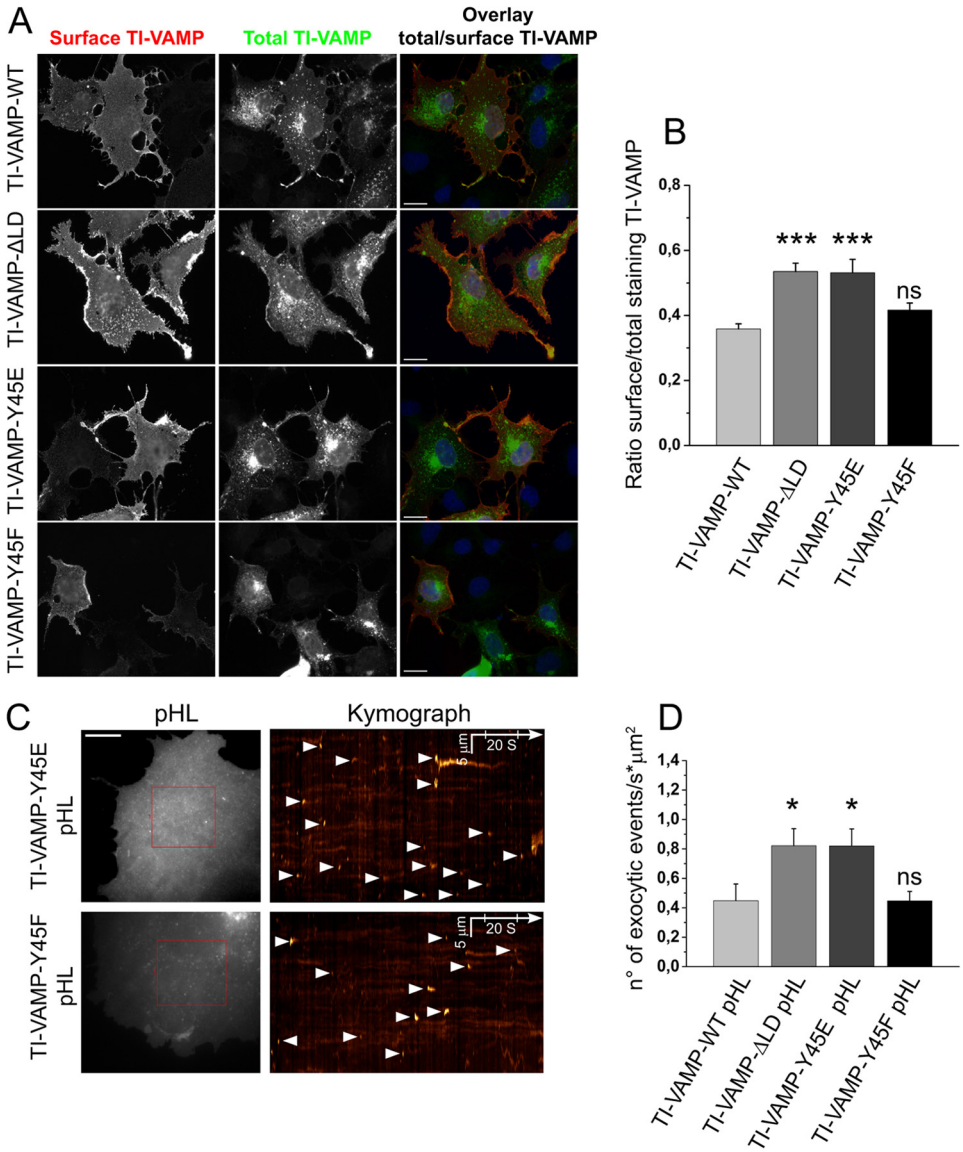

FIGURE 5. **Mutation of Tyr-45 into glutamate but not phenylalanine of the TI-VAMP LD regulates TI-VAMP localization and its mediated exocytosis in COS-7 cells.** COS-7 cells were transfected with TI-VAMP-WT, -ΔLD, -Y45E, or -Y45F pHL and processed for surface immunostaining or imaged live after 16–24 h. *A*, cells were chosen on the basis of total TI-VAMPs pHL expression (*green*) and processed for quantification of TI-VAMP pHL (*red*) surface staining. The ratio between *red* and *green* staining (overlay) was calculated to evaluate the rate of TI-VAMP exocytosis in the different experimental conditions. *Scale bar*, 20 μm. *B*, quantification of the ratio between surface and total expressed TI-VAMP pHL staining (see "Experimental Procedures"). *C*, exocytosis of TI-VAMP pHL constructs was monitored by fast time lapse video imaging, quantified as described under "Experimental Procedures." The more relevant exocytic events, here represented by kymograph (see also supplemental Movie S2), appear as bright spots (*arrowheads*). *Scale bar*, 10 μm (*left panels*). *D*, quantification of the density per second of exocytic events for TI-VAMP constructs. The data are shown as the means ± S.E. Significance was determined by one-way ANOVA, Dunnett's post test. *, $p < 0.05$; ***, $p < 0.001$; *ns*, not significant.

t-SNARE partners is regulated by the introduction of a negative charge mimicking the phosphorylation of Tyr-45. This mutation likely increases accessibility of TI-VAMP SNARE domain to t-SNARE partners similar to LD deletion.

Y45E Mutation Increases TI-VAMP Exocytosis—Removal of LD was previously shown to activate exocytosis of TI-VAMP and increase the presence of the v-SNARE at the plasma membrane, most likely as the result of t-SNARE binding activation (11) and loss of interaction with Hrb (23, 41). Thus, we investigated whether the introduction of a negative charge at the residue Tyr-45 is also able to induce alterations in TI-VAMP distribution. To this aim, we analyzed the amount of TI-VAMP at the cell surface and its rate of exocytosis in COS-7 cells expressing the different TI-VAMP mutants fused to pHL (Fig. 5*A*). Quantification of surface staining allowed us to detect the fraction of TI-VAMP that had accumulated at the cellular plasma membrane, with respect to the total amount of the expressed protein. As expected, LD deletion promoted a strong increase in the concentration of TI-VAMP at the plasma membrane, with respect to the wild type form, confirming the autoinhibitory and endocytic roles of LD (Fig. 5*B*). Y45E induced increased cell surface staining similarly to ΔLD, whereas Y45F was similar to WT. We further analyzed the role of Tyr-45 on TI-VAMP exocytosis in live cells (3). COS-7 cells were transfected with TI-VAMP-WT, -ΔLD, -Y45E, and -Y45F pHL constructs, and the exocytic events were monitored by time lapse

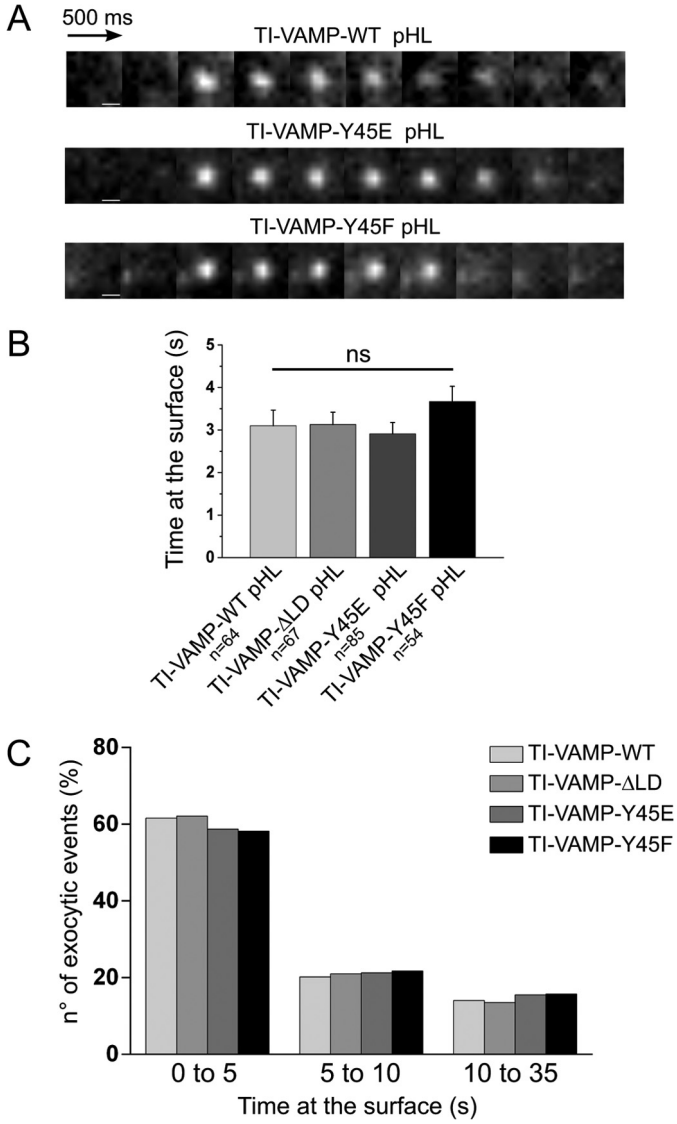

FIGURE 6. **TI-VAMP exocytosis kinetics is independent on LD deletion and Tyr-45 mutation.** COS-7 cells were transfected with TI-VAMP-WT, -ΔLD, -Y45E, or -Y45F pHL. After 16–24 h, the exocytosis of TI-VAMP pHL constructs was monitored by fast time lapse video imaging. Individual exocytic event appears as diffraction-limited "puffs" of TI-VAMP pHL fluorescence that differed in kinetics. Some TI-VAMP pHLs puffs dissipated quickly (0.5 s), and others remained for a more prolonged time period (>10 s), dissipating gradually over this time period. *A*, representative snapshots of individual exocytic event for TI-VAMP-WT, -Y45E, and -Y45F pHL with similar kinetics. *Scale bars*, 500 nm. *B*, quantification of TI-VAMP pHL construct exocytic kinetics. Kinetics of each individual TI-VAMP pHL puff was quantified by measuring the interval time between its appearance and its dissipation. *n*, number of individual exocytic event analyzed. *ns*, not significant. *C*, quantification of WT and mutant TI-VAMP pHL exocytic kinetics using custom-written scripts in FIJI and Matlab software (see "Experimental Procedures"). Frequency distribution (%) of different temporal classes of TI-VAMP mutants exocytic events (0–5, short; 5–10, intermediate; 10–35, long) are indicated on the *abscissa*.

video microscopy (Fig. 5*C* and supplemental Movie S2). As expected, LD deletion induced an increased rate of TI-VAMP exocytosis compared with TI-VAMP-WT (Fig. 5*D*) in accord with previous results (5). In agreement with surface staining, Y45E significantly increased the rate of TI-VAMP exocytosis, whereas Y45F was similar to WT. We did not find any effect on the kinetics of pHL puffs (Fig. 6, *A* and *B*) with a time average at the surface of ~3 s for all the TI-VAMP constructs, suggesting that pore opening is likely not drastically changed by Tyr-45 mutations or LD deletion. These later data are in agreement with the fundamental role of SNARE domain to drive membrane fusion. Analysis of TI-VAMPs pHL movies suggested that TI-VAMP exocytosis was characterized by both a predominant transient mode characterized by transient flashes of light and a persistent mode with relative long lasting fluorescent spots (irregular bright lines in kymograph). Interestingly these two alternative modes have been described previously for the exocytosis of β2 adrenergic receptor in hippocampal neurons (42). To evaluate whether TI-VAMP mutants have an overall or specific effect in some subpopulation of TI-VAMP vesicles, we measured the time spent at the surface for each exocytic events in COS-7 cells expressing TI-VAMP-pHL mutants (see "Experimental Procedures"). As shown in Fig. 6*C*, all the mutants have the same frequency distribution of short- and long-lived exocytic events, suggesting that LD deletion and the Y45E mutant increase overall the frequency of TI-VAMP exocytosis. Taken together, these results show that the introduction of a negative charge at Tyr-45 enhances translocation of TI-VAMP to the plasma membrane and exocytosis rate.

Because Tyr-45 is involved in binding of Hrb, which mediates clathrin-dependent endocytosis of TI-VAMP (23, 41), its mutation could prevent Hrb-mediated efficient endocytosis. Unfortunately the low affinity of TI-VAMP/Hrb interaction (23) prevented further investigation of the precise molecular effect of Tyr-45 mutations on endocytosis. However, despite probable perturbation of TI-VAMP/Hrb interaction, we found that Y45F and Y45E mutants still co-localized to a great extent with TI-VAMP-WT (Fig. 7, *A* and *B*), suggesting that Y45E is likely to enhance exocytosis without any effect on endocytosis and intracellular localization. Moreover, the expression of these TI-VAMP mutants did not affect the density or the average size of TI-VAMP vesicles (Fig. 7, *C* and *D*), indicating that the pool of vesicles of WT and the mutants is similar. Altogether, these data suggest that the main effect of Y45E mutation is to enhance the SNARE activity of TI-VAMP.

Y45E Mutation Induces Both an Increase of Axonal Growth and Exocytosis in Hippocampal Neurons—It has been previously shown that TI-VAMP plays a role in neurite growth and that its LD has a negative role in this process in cultured neuronal cells (10, 28, 43). Thus, we investigated whether or not Tyr-45 mutations altered neurite growth. Rat hippocampal neurons were transfected with TI-VAMP mutants at 2 DIV, and the axonal length (the longest MAP2 negative neurite) was measured after 24 h (Fig. 8*A*). Compared with the TI-VAMP-WT pHL transfection, hippocampal neurons expressing TI-VAMP-ΔLD pHL showed a higher neurite elongation as previously demonstrated (10) (Fig. 8*B*). Accordingly, Y45E mutant induced a ΔLD-like stimulation, whereas the Y45F substitution did not alter axonal growth compared with WT. These data suggest that a negative charge replacing Tyr-45 leads to a positive modulation of TI-VAMP in cultured neurons. We further analyzed the role of Tyr-45 mutations by live imaging of TI-VAMP exocytosis in the cell body of hippocampal neurons at 3 DIV (3) (Fig. 8*C* and supplemental Movie S3). As in COS-7 cells, both TI-VAMP-ΔLD and -Y45E pHL mutants showed an increased rate of exocytosis, whereas TI-VAMP-Y45F had no

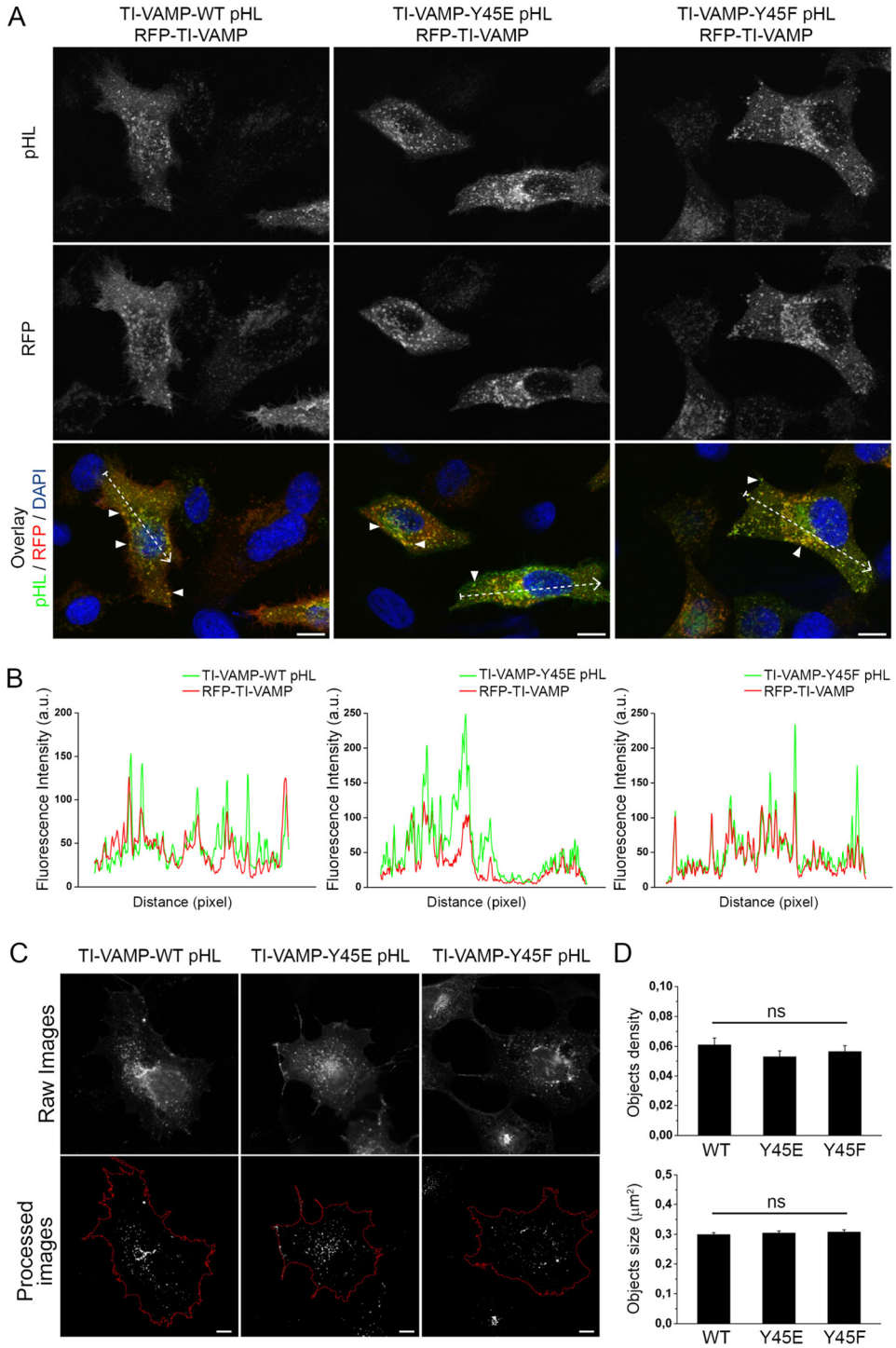

FIGURE 7. **Y45F and Y45E mutations do not alter the subcellular localization, density, and size of TI-VAMP vesicles.** *A*, HeLa cells were co-transfected with TI-VAMP-WT, -Y45E, or -Y45F pHL and RFP-TI-VAMP. TI-VAMP pHL (*green*) and RFP-TI-VAMP (*red*) were detected by indirect immunofluorescence using specific GFP and RFP antibodies. Overlay shows co-localization between the different TI-VAMP pHL constructs and RFP-TI-VAMP. *Arrowheads* point to vesicular structures containing both TI-VAMP pHL and RFP-TI-VAMP. *Scale bar*, 10 μm. RFP, red fluorescent protein. *B*, line scans from the *dotted lines* traced in the overlay images representing the co-localization between TI-VAMP pHL constructs and RFP TI-VAMP. *a.u.*, arbitrary units. *C* and *D*, quantification of TI-VAMP membrane structures number (objects density, *C*) and size (*D*) per cell. COS-7 cells were transfected with TI-VAMP-WT ($n = 18$), TI-VAMP-Y45E ($n = 18$), or TI-VAMP-Y45F ($n = 17$) pHL and processed for immunofluorescence. The images were analyzed as described under "Experimental Procedures" to obtain the total number of TI-VAMPs GFP positive vesicles per cell (object density) and their size. Significance was determined by one-way ANOVA, Dunnett's post test. *ns*, not significant.

effect (Fig. 8*D*). Altogether, these results show that the introduction of a negative charge mimicking a phosphorylation of TI-VAMP Tyr-45 increases both axonal length and exocytic rate in rat hippocampal neurons, thus producing the activation expected when LD autoinhibition is released.

DISCUSSION

Here we showed first that insulin and IGF-1, two upstream activators of the c-Src pathway, positively regulate the activity of TI-VAMP by inducing a rise in its frequency of exocytosis. Second, we found that TI-VAMP is phosphorylated in its LD on

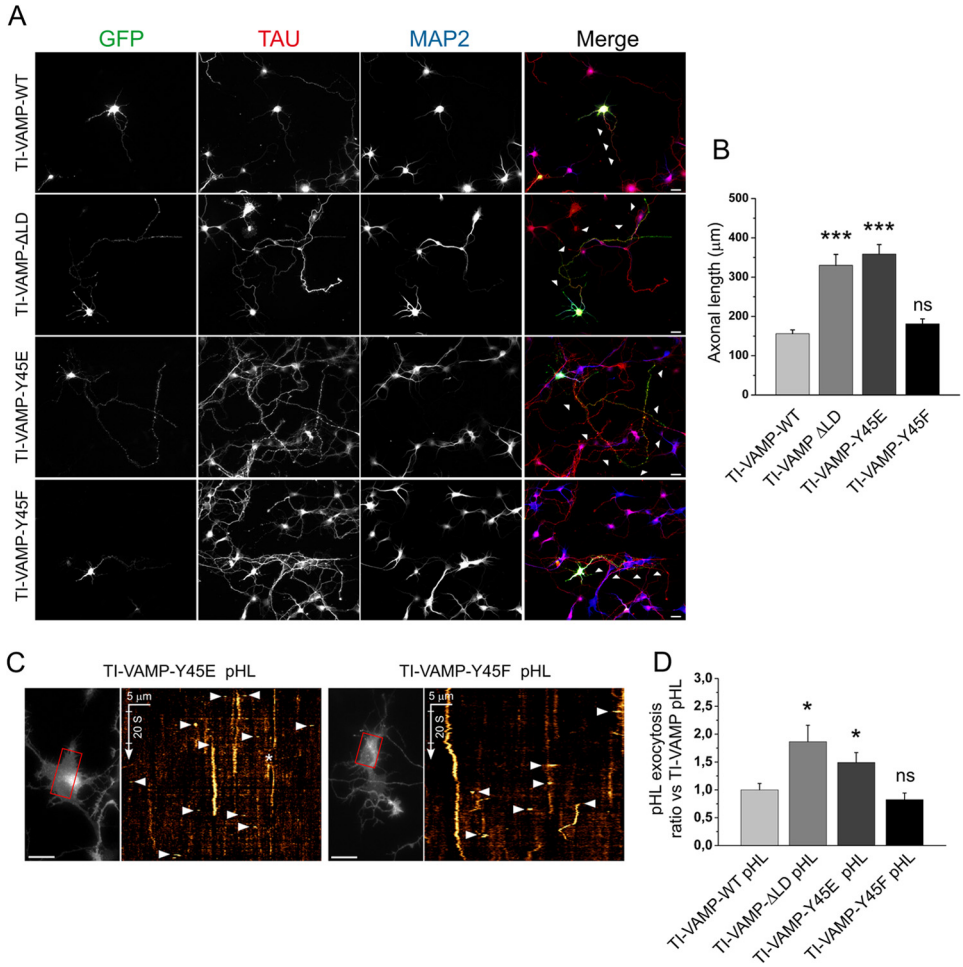

FIGURE 8. **The Y45E substitution increases axonal length and TI-VAMP-mediated exocytosis in hippocampal neurons.** Rat hippocampal neurons were transfected at 2 DIV with TI-VAMP-WT, -ΔLD, -Y45E, or -Y45F pHL and processed for immunofluorescence or imaged live after 24 h. *A* and *B*, TI-VAMP-Y45E increases axonal length. *A*, after fixation neurons were labeled for GFP (*green*), axonal (Tau, *red*), and dendritic (MAP2, *blue*) markers. *Scale bars*, 20 μm. *B*, quantification of the axonal length (*arrowheads*) in transfected neurons. *C* and *D*, Y45E mutation increases TI-VAMP-mediated exocytosis. Rat hippocampal neurons were transfected with TI-VAMP pHL constructs at 2 DIV and imaged live at 3 DIV. *C*, exocytic events of TI-VAMP pHL constructs in the cell body (in *red boxes*) were quantified as described under "Experimental Procedures." The more relevant exocytic events, here visualized by kymograph (see also supplemental Movie S3), appear as bright spots (*arrowheads*). *, exocytic event not quantified. *Scale bars*, 20 μm (*left panels*). *D*, quantification of exocytic events for TI-VAMP constructs. The data are represented as ratios between the densities per second of exocytic events of TI-VAMP mutants and TI-VAMP-WT and showed as the means ± S.E. Significance was determined by one-way ANOVA, Dunnett's post test. *, $p < 0.05$; ***, $p < 0.001$; *ns*, not significant.

Tyr-45 and, more specifically, that this event is mediated by c-Src. Thus, we conclude that TI-VAMP is a c-Src substrate and suggest that c-Src phosphorylation regulates TI-VAMP-mediated exocytosis by removing the LD autoinhibition. According to these new results and previous results showing that c-Src inhibition decreases the frequency of TI-VAMP exocytic events in cortical neurons (28), we suggest that the role of TI-VAMP in neurite growth may be tightly link to c-Src-dependent pathways, potentially downstream of insulin/IGF-1 (this study), integrin activation (28), and potentially other plasma membrane receptors, rather than a general regulator mechanism. Moreover, in mature synapses, TI-VAMP was already proposed to regulate exocytosis of the resting pool of synaptic vesicles (5). In this context, our data suggest that c-Src phosphorylation of TI-VAMP may activate the exocytosis of this resting pool, potentially independently of depolarization. It is also known that TI-VAMP is expressed at a high level in subsets of nerve terminals (19) and particularly in mossy fiber nerve terminals. Thus, an expected consequence of this study together with previous ones (4, 5) is that a form of neurotransmitter release could be activated by a c-Src-dependent signaling pathway in mossy fiber nerve terminals. c-Src was found to play an important role in vesiculation at the Golgi (37) and to associate with synaptic vesicles (44); thus, it could be a regulator of a specific subset of secretory vesicles that use TI-VAMP for their exocytosis (2, 3).

The LD of TI-VAMP has been proven to play a crucial role in the regulation of TI-VAMP, through its autoinhibitory molecular function (10, 11). Recently, it has been shown that TI-VAMP adopts a stable, closed conformation in solution and that its stability depends on the hydrophobic interaction between the LD and the SNARE core (12). Up to now, two amino acids, Leu-43 and Tyr-45, have been shown to play a role in the acquisition of the closed conformation of TI-VAMP (24) and also the interactions with Hrb and AP-3 (23, 40), thus coordinating its function as a v-SNARE and intracellular sorting. We further showed here that the insertion of a negative charge in place of Tyr-45 induces an increase in its biological activity *in vitro* and *in vivo*. Indeed, we demonstrated that the binding

affinity between TI-VAMP and Syntaxin-1/SNAP-25 complex *in vitro* is increased by introduction of phospho-mimetic residue replacing Tyr-45. When the Y45E mutant of TI-VAMP is expressed in COS-7 cells and neurons, a rise in the level of TI-VAMP-mediated exocytosis was observed, together with a relevant increase in the plasma membrane translocation. Additionally, we demonstrated that the Y45E mutation leads to an increment in neurite elongation, with a ΔLD-like effect, in rat hippocampal neurons in primary culture. Altogether, these data suggest that the presence of a negative moiety in the Tyr-45 position may participate to disrupt the LD-SNARE core contact region, favoring both a structural detachment of the two domains and an interaction between the TI-VAMP SNARE core and the t-SNARE partners. It remains to be determined whether other molecular mechanisms, possibly involving other TI-VAMP partners, may also participate to trigger TI-VAMP opening and whether Tyr-45 acts secondarily to stabilize this open conformation.

In conclusion, our findings allow positioning TI-VAMP as a potential effector of c-Src- and insulin/IGF-1-dependent signaling pathways. Whether or not these are the only activatory pathways of TI-VAMP-dependent exocytosis is an open question. In addition, the possible links between c-Src and insulin/IGF-1 in membrane trafficking regulation still remain to be investigated. In this context, it is intriguing that both c-Src (45) and IGF-1R (46) have been found to regulate the Golgi apparatus, the main source of TI-VAMP secretory vesicles (3).

Acknowledgments—We are grateful to imaging facility of the Institut Jacques Monod. We are grateful to the Galli laboratory for helpful discussions.

REFERENCES

1. Filippini, F., Rossi, V., Galli, T., Budillon, A., D'Urso, M., and D'Esposito, M. (2001) Longins. A new evolutionary conserved VAMP family sharing a novel SNARE domain. *Trends Biochem. Sci* **26,** 407–409
2. Chaineau, M., Danglot, L., and Galli, T. (2009) Multiple roles of the vesicular-SNARE TI-VAMP in post-Golgi and endosomal trafficking. *FEBS Lett.* **583,** 3817–3826
3. Burgo, A., Proux-Gillardeaux, V., Sotirakis, E., Bun, P., Casano, A., Verraes, A., Liem, R. K., Formstecher, E., Coppey-Moisan, M., and Galli, T. (2012) A molecular network for the transport of the TI-VAMP/VAMP7 vesicles from cell center to periphery. *Dev. Cell* **23,** 166–180
4. Scheuber, A., Rudge, R., Danglot, L., Raposo, G., Binz, T., Poncer, J. C., and Galli, T. (2006) Loss of AP-3 function affects spontaneous and evoked release at hippocampal mossy fiber synapses. *Proc. Natl. Acad. Sci. U.S.A.* **103,** 16562–16567
5. Hua, Z., Leal-Ortiz, S., Foss, S. M., Waites, C. L., Garner, C. C., Voglmaier, S. M., and Edwards, R. H. (2011) v-SNARE composition distinguishes synaptic vesicle pools. *Neuron* **71,** 474–487
6. Danglot, L., Zylbersztejn, K., Petkovic, M., Gauberti, M., Meziane, H., Combe, R., Champy, M. F., Birling, M. C., Pavlovic, G., Bizot, J. C., Trovero, F., Della Ragione, F., Proux-Gillardeaux, V., Sorg, T., Vivien, D., D'Esposito, M., and Galli, T. (2012) Absence of TI-VAMP/Vamp7 leads to increased anxiety in mice. *J. Neurosci.* **32,** 1962–1968
7. Verderio, C., Cagnoli, C., Bergami, M., Francolini, M., Schenk, U., Colombo, A., Riganti, L., Frassoni, C., Zuccaro, E., Danglot, L., Wilhelm, C., Galli, T., Canossa, M., and Matteoli, M. (2012) TI-VAMP/VAMP7 is the SNARE of secretory lysosomes contributing to ATP secretion from astrocytes. *Biol. Cell* **104,** 213–228
8. Fader, C. M., Aguilera, M. O., and Colombo, M. I. (2012) ATP is released from autophagic vesicles to the extracellular space in a VAMP7-dependent manner. *Autophagy* **8,** 1741–1756
9. Danglot, L., Chaineau, M., Dahan, M., Gendron, M.-C., Boggetto, N., Perez, F., and Galli, T. (2010) Role of TI-VAMP and CD82 in EGFR cell-surface dynamics and signaling. *J. Cell Sci.* **123,** 723–735
10. Martinez-Arca, S., Alberts, P., Zahraoui, A., Louvard, D., and Galli, T. (2000) Role of tetanus neurotoxin insensitive vesicle-associated membrane protein (TI-VAMP) in vesicular transport mediating neurite outgrowth. *J. Cell Biol.* **149,** 889–900
11. Martinez-Arca, S., Rudge, R., Vacca, M., Raposo, G., Camonis, J., Proux-Gillardeaux, V., Daviet, L., Formstecher, E., Hamburger, A., Filippini, F., D'Esposito, M., and Galli, T. (2003) A dual mechanism controlling the localization and function of exocytic v-SNAREs. *Proc. Natl. Acad. Sci. U.S.A.* **100,** 9011–9016
12. Vivona, S., Liu, C. W., Strop, P., Rossi, V., Filippini, F., and Brunger, A. T. (2010) The longin SNARE VAMP7/TI-VAMP adopts a closed conformation. *J. Biol. Chem.* **285,** 17965–17973
13. Gerst, J. E. (2003) SNARE regulators. Matchmakers and matchbreakers. *Biochim. Biophys. Acta* **1641,** 99–110
14. Snyder, D. A., Kelly, M. L., and Woodbury, D. J. (2006) SNARE complex regulation by phosphorylation. *Cell Biochem. Biophys.* **45,** 111–123
15. Gurd, J. W. (1997) Protein tyrosine phosphorylation. Implications for synaptic function. *Neurochem. Int.* **31,** 635–649
16. Shimazaki, Y., Nishiki, T., Omori, A., Sekiguchi, M., Kamata, Y., Kozaki, S., and Takahashi, M. (1996) Phosphorylation of 25-kDa synaptosome-associated protein. Possible involvement in protein kinase C-mediated regulation of neurotransmitter release. *J. Biol. Chem.* **271,** 14548–14553
17. Rickman, C., and Duncan, R. R. (2010) Munc18/Syntaxin interaction kinetics control secretory vesicle dynamics. *J. Biol. Chem.* **285,** 3965–3972
18. Burgo, A., Sotirakis, E., Simmler, M. C., Verraes, A., Chamot, C., Simpson, J. C., Lanzetti, L., Proux-Gillardeaux, V., and Galli, T. (2009) Role of Varp, a Rab21 exchange factor and TI-VAMP/VAMP7 partner, in neurite growth. *EMBO Rep.* **10,** 1117–1124
19. Muzerelle, A., Alberts, P., Martinez-Arca, S., Jeannequin, O., Lafaye, P., Mazié, J.-C., Galli, T., and Gaspar, P. (2003) Tetanus neurotoxin-insensitive vesicle-associated membrane protein localizes to a presynaptic membrane compartment in selected terminal subsets of the rat brain. *Neuroscience* **122,** 59–75
20. McNew, J. A., Weber, T., Parlati, F., Johnston, R. J., Melia, T. J., Söllner, T. H., and Rothman, J. E. (2000) Close is not enough. SNARE-dependent membrane fusion requires an active mechanism that transduces force to membrane anchors. *J. Cell Biol.* **150,** 105–117
21. Fevrier, B., Vilette, D., Archer, F., Loew, D., Faigle, W., Vidal, M., Laude, H., and Raposo, G. (2004) Cells release prions in association with exosomes. *Proc. Natl. Acad. Sci. U.S.A.* **101,** 9683–9688
22. Danglot, L., Triller, A., and Bessis, A. (2003) Association of gephyrin with synaptic and extrasynaptic GABAA receptors varies during development in cultured hippocampal neurons. *Mol. Cell. Neurosci.* **23,** 264–278
23. Pryor, P. R., Jackson, L., Gray, S. R., Edeling, M. A., Thompson, A., Sanderson, C. M., Evans, P. R., Owen, D. J., and Luzio, J. P. (2008) Molecular basis for the sorting of the SNARE VAMP7 into endocytic clathrin-coated vesicles by the ArfGAP Hrb. *Cell* **134,** 817–827
24. Schäfer, I. B., Hesketh, G. G., Bright, N. A., Gray, S. R., Pryor, P. R., Evans, P. R., Luzio, J. P., and Owen, D. J. (2012) The binding of Varp to VAMP7 traps VAMP7 in a closed, fusogenically inactive conformation. *Nat. Struct. Mol. Biol.* **19,** 1300–1309
25. Winn, M. D., Murshudov, G. N., and Papiz, M. Z. (2003) Macromolecular TLS refinement in Refmac at moderate resolutions. *Methods Enzymol.* **374,** 300–321
26. Weber, T., Zemelman, B. V., McNew, J. A., Westermann, B., Gmachl, M., Parlati, F., Söllner, T. H., and Rothman, J. E. (1998) SNAREpins. Minimal machinery for membrane fusion. *Cell* **92,** 759–772
27. Sankaranarayanan, S., and Ryan, T. A. (2000) Real-time measurements of vesicle-SNARE recycling in synapses of the central nervous system. *Nat Cell Biol.* **2,** 197–204
28. Gupton, S. L., and Gertler, F. B. (2010) Integrin signaling switches the cytoskeletal and exocytic machinery that drives neuritogenesis. *Dev. Cell* **18,** 725–736

29. Blakesley, V. A., Scrimgeour, A., Esposito, D., and Le Roith, D. (1996) Signaling via the insulin-like growth factor-I receptor. Does it differ from insulin receptor signaling? *Cytokine Growth Factor Rev.* **7,** 153–159
30. Randhawa, V. K., Thong, F. S., Lim, D. Y., Li, D., Garg, R. R., Rudge, R., Galli, T., Rudich, A., and Klip, A. (2004) Insulin and hypertonicity recruit GLUT4 to the plasma membrane of muscle cells using NSF-dependent SNARE mechanisms but different v-SNAREs. Role of TI-VAMP. *Mol. Biol. Cell* **15,** 5565–5573
31. Bondy, C. A., and Cheng, C. M. (2004) Signaling by insulin-like growth factor 1 in brain. *Eur. J. Pharmacol.* **490,** 25–31
32. Zhao, W. Q., and Alkon, D. L. (2001) Role of insulin and insulin receptor in learning and memory. *Mol. Cell. Endocrinol.* **177,** 125–134
33. Chiu, S. L., and Cline, H. T. (2010) Insulin receptor signaling in the development of neuronal structure and function. *Neural Dev.* **5,** 7
34. Plum, L., Schubert, M., and Brüning, J. C. (2005) The role of insulin receptor signaling in the brain. *Trends Endocrinol. Metab.* **16,** 59–65
35. Zhao, W., Cavallaro, S., Gusev, P., and Alkon, D. L. (2000) Nonreceptor tyrosine protein kinase pp60c-src in spatial learning. Synapse-specific changes in its gene expression, tyrosine phosphorylation, and protein-protein interactions. *Proc. Natl. Acad. Sci. U.S.A.* **97,** 8098–8103
36. Luttrell, L. M., Luttrell, D. K., Parsons, S. J., and Rogol, A. D. (1989) Insulin and phorbol ester induce distinct phosphorylations of pp60c-src in the BC3H-1 murine myocyte cell line. *Oncogene* **4,** 317–324
37. Weller, S. G., Capitani, M., Cao, H., Micaroni, M., Luini, A., Sallese, M., and McNiven, M. A. (2010) Src kinase regulates the integrity and function of the Golgi apparatus via activation of dynamin 2. *Proc. Natl. Acad. Sci. U.S.A.* **107,** 5863–5868
38. Cao, H., Chen, J., Krueger, E. W., and McNiven, M. A. (2010) SRC-mediated phosphorylation of dynamin and cortactin regulates the "constitutive" endocytosis of transferrin. *Mol. Cell. Biol.* **30,** 781–792
39. Nada, S., Okada, M., MacAuley, A., Cooper, J. A., and Nakagawa, H. (1991) Cloning of a complementary DNA for a protein-tyrosine kinase that specifically phosphorylates a negative regulatory site of p60c-src. *Nature* **351,** 69–72
40. Kent, H. M., Evans, P. R., Schäfer, I. B., Gray, S. R., Sanderson, C. M., Luzio, J. P., Peden, A. A., and Owen, D. J. (2012) Structural basis of the intracellular sorting of the SNARE VAMP7 by the AP3 adaptor complex. *Dev. Cell* **22,** 979–988
41. Chaineau, M., Danglot, L., Proux-Gillardeaux, V., and Galli, T. (2008) Role of HRB in clathrin-dependent endocytosis. *J. Biol. Chem.* **283,** 34365–34373
42. Yudowski, G. A., Puthenveedu, M. A., and von Zastrow, M. (2006) Distinct modes of regulated receptor insertion to the somatodendritic plasma membrane. *Nat. Neurosci.* **9,** 622–627
43. Martinez-Arca, S., Coco, S., Mainguy, G., Schenk, U., Alberts, P., Bouillé, P., Mezzina, M., Prochiantz, A., Matteoli, M., Louvard, D., and Galli, T. (2001) A common exocytotic mechanism mediates axonal and dendritic outgrowth. *J. Neurosci.* **21,** 3830–3838
44. Linstedt, A. D., Vetter, M. L., Bishop, J. M., and Kelly, R. B. (1992) Specific association of the proto-oncogene product pp60c-src with an intracellular organelle, the PC12 synaptic vesicle. *J. Cell Biol.* **117,** 1077–1084
45. Bard, F., Mazelin, L., Péchoux-Longin, C., Malhotra, V., and Jurdic, P. (2003) Src regulates Golgi structure and KDEL receptor-dependent retrograde transport to the endoplasmic reticulum. *J. Biol. Chem.* **278,** 46601–46606
46. Chia, J., Goh, G., Racine, V., Ng, S., Kumar, P., and Bard, F. (2012) RNAi screening reveals a large signaling network controlling the Golgi apparatus in human cells. *Mol. Syst. Biol.* **8,** 629
47. Amanchy, R., Periaswamy, B., Mathivanan, S., Reddy, R., Tattikota, S. G., and Pandey, A. (2007) A curated compendium of phosphorylation motifs. *Nat. Biotechnol.* **25,** 285–286
48. Huang, P., Altshuller, Y. M., Hou, J. C., Pessin, J. E., and Frohman, M. A. (2005) Insulin-stimulated plasma membrane fusion of Glut4 glucose transporter-containing vesicles is regulated by phospholipase D1. *Mol. Biol. Cell* **16,** 2614–2623
49. Blom, N., Gammeltoft, S., and Brunak, S. (1999) Sequence and structure-based prediction of eukaryotic protein phosphorylation sites. *J. Mol. Biol.* **294,** 1351–1362
50. Blom, N., Sicheritz-Pontén, T., Gupta, R., Gammeltoft, S., and Brunak, S. (2004) Prediction of post-translational glycosylation and phosphorylation of proteins from the amino acid sequence. *Proteomics* **4,** 1633–1649
51. Xue, Y., Ren, J., Gao, X., Jin, C., Wen, L., and Yao, X. (2008) GPS 2.0, a tool to predict kinase-specific phosphorylation sites in hierarchy. *Mol. Cell. Proteomics* **7,** 1598–1608